# Preliminary experimental study and simulation of an energy-tunable quasi-monochromatic laser-Compton X/γ-ray source*

LUO Wen(罗文)[1,2,3;1)] XU Wang(徐望)[2] ZHUO Hong-Bin(卓红斌)[3;2)] MA Yan-Yun(马燕云)[3]

[1] College of Nuclear Science and Technology, University of South China, Hengyang 421001, China
[2] Shanghai Institute of Applied Physics, Chinese Academy of Sciences, Shanghai 201800, China
[3] College of Science, National University of Defense Technology, Changsha 410073, China

**Abstract:** We propose a slanting collision scheme for Compton scattering of a laser light against a relativistic electron beam. This scheme is suitable to generate an energy-tunable X/γ-ray source. In this paper, we present theoretical study and simulation of the spectral, spatial and temporal characteristics of such a source. We also describe two terms laser-Compton scattering (LCS) experiments at the 100 MeV Linac of Shanghai Institute of Applied Physics, where quasi-monochromatic LCS X-ray energy spectra with peak energies of ∼30 keV are observed successfully. These preliminary investigations are carried out to understand the feasibility of developing an energy-tunable quasi-monochromatic X/γ-ray source, the future Shanghai Laser Electron Gamma Source.

**Key words:** energy-tunable, LCS, slanting collision, X/γ-ray

**PACS:** 29.27.-a, 13.60.Fz, 07.85.Fv **DOI:** 10.1088/1674-1137/36/8/016

## 1 Introduction

Rapid advances in terawatt-class laser technology [1] and high-brightness, high-gradient electron accelerators [2] are enabling the development of a new type of light source based on Compton/Thomson scattering [3, 4], where relativistic electrons interact with a coherent photon field to generate bright, ultrafast, and ultrashort X/γ-rays [5–9]. This kind of source (denoted as laser-Compton scattering (LCS) X/γ-ray source) is a natural complement to the large-scale 3rd and 4th generation light sources [10], and provides a means to generate MeV-scale photons [11] with unprecedented spectral brightness. As an example, the Tsinghua Thomson-scattering X-ray Source [9, 12] is proposed and under construction with a linac and a compact storage ring at the electron energy of 40–50 MeV.

Among other important features, LCS X/γ-ray source offers the potential of generating energy-tunable and quasi-monochromatic radiation in a very small solid angle. These characteristics are suitable not only for the calibration of γ-ray detectors (including the Compton telescope, pair telescopes, Si trip detectors and scintillator calorimeters) in aerospace [13, 14], but also for studies in the field of nuclear physics and nuclear astrophysics [15, 16]. Moreover, as an important potential application of this source, we point out the detection of hidden special nuclear materials with the nuclear resonance fluorescence (NRF) method [17]. Due to the fact that the width of nuclear resonance is quite narrow (⩽eV) and the overwhelming fraction of gamma-rays outside the resonance window contributes unwanted background, a monochromatic and tunable γ-ray beam is indispensable to obtain precise data with a good signal-to-noise ratio in NRF.

Usually, a collimator scheme is used to produce a

Received 18 October 2011

* Supported by One Hundred Talents Project of the Chinese Academy of Sciences (2006) (26010701), Knowledge Innovation Project of Chinese Academy of Sciences (KJCX2-SW-N13) and National Natural Science Foundation of China (10976031, 10835003, 11175253, 11175254)

1) E-mail: wenluo-ok@163.com

2) E-mail: hongbin.zhuo@gmail.com

quasi-monochromatic X/γ-ray beam in an energy range of ⩽100 MeV. The available methods to generate a tunable X/γ-ray beam are (1) changing the electron beam energy, (2) using a tunable laser, (3) choosing a scattered angle of the laser-Compton X/γ-rays by using a collimator, and (4) selecting a collision angle of the laser-electron interaction (i.e. slanting LCS scheme). In most cases, the electron energies employed for the LCS process can hardly be adjusted, such as the fixed electron energies at the storage ring for synchrotron radiation. Since a tunable laser with an optical parametric oscillator does not have enough power in the infrared wavelength region, an intense gamma-ray beam cannot presently be generated by using a tunable laser, but may be a potential method in the near future. A collimator-absorber method is employed by Ohgake et al. [18] to select the scattered angle of the laser-Compton X/γ-rays and then to obtain energy-tunable γ-rays. However, the results show a relatively broad energy spread, 7 % - 9 %, and a narrow tuned energy range. When a slanting LCS scheme is employed with the laser incident angle varying from about 20° to 180° (i.e. head-on collision), a broad energy of the X/γ-ray beam will be tuned from ⩽10 keV to sub-MeV if 100 MeV electron beams collide with 0.8 μm laser pulses.

Therefore, we propose an acceptable method: a slanting LCS scheme to generate an energy-tunable X/γ-ray beam where the laser pulse duration and timing are synchronized with the electron beam pulse. Recently, utilizing this scheme we have performed two terms X-ray production experiments at the 100 MeV Linac of the Shanghai Institute of Applied Physics (SINAP), denoted as SINAP Ⅰ [19] and SINAP Ⅱ [20]. The main purpose for these two experiments is to address some technical issues concerning the construction of a quasi-monochromatic γ-ray source with a tunable-energy from MeV to hundreds MeV, i.e. the proposed Shanghai Laser Electron Gamma Source (SLEGS) [21] at the Shanghai Synchrotron Radiation Facility. Meanwhile, the capability of accurately predicting the spatial, spectral and temporal characteristics of a laser-Compton light source is crucial for its optimized design, as well as for future experiments and applications utilizing such sources. With this motivation and consideration, a 4D (three dimensional time and frequency-domain) Monte Carlo laser-Compton scattering simulation code (MCLCSS) [22] has been developed with the Geant4 toolkit [23]. For the first time, this code has the ability to model a slanting LCS scheme, and fully take into account the effects of incoming beam parameters and the effects of X/γ-ray beam collimation and transportation.

In this work, we describe theoretically the main characteristics of an LCS X/γ-ray beam within the slanting interaction scheme (see Section 2). Then we summarize two terms LCS experiments performed at SINAP (see Section 3). Later we study the spectral, spatial and temporal characteristics of the Compton gamma-ray beam using our newly developed code, 4D-MCLCSS (see Section 4). Finally, we present a summary and outlook (see Section 5).

## 2 Theoretical descriptions for a slanting LCS scheme

A typical LCS process in the laboratory frame is shown in Fig. 1. An electron bunch is moving along the $z$-axis and a laser pulse is propagated along a direction with an incident angle of $\theta_{\rm L}$ with respect to the $z$-axis. When an incident laser photon of energy $E_{\rm L}$ strikes an electron of energy $E_{\rm e}$ and velocity $\beta$, the energy of the LCS X/γ-ray in the plane of incidence (defined by the incident laser and electron beam directions) is given by

$$E_{\rm p}=\frac{E_{\rm L}(1-\beta\cos\theta_{\rm L})}{(1-\beta\cos\theta)+\dfrac{E_{\rm L}}{E_{\rm e}}\gamma^2(1-\beta)(1+\cos\theta)(1-\beta\cos\theta_{\rm L})}. \tag{1}$$

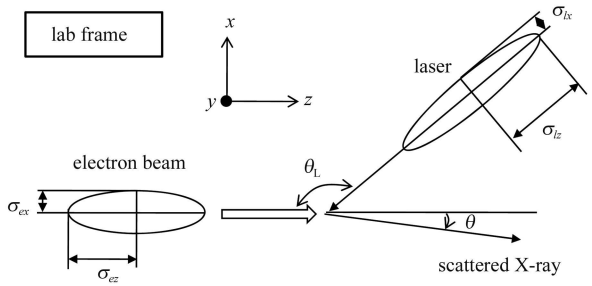


Fig. 1. The coordinates for LCS between a relativistic electron and laser photon in the laboratory frame.

Here, $\theta$ is the scattered angle of the LCS photon with respect to the direction of the incident electron beam, and $\gamma$ is the electron Lorentz factor. As an example, we show a 3D-plot of the LCS X/γ-ray energy against the incident angle $\theta_{\rm L}$ and scattered angle $\theta$ (see Fig. 2). In a case of a 1064 nm laser pulse brought to a slanting collision at 40° with a 112 MeV electron beam, the forward radiated X-rays have a maximum energy of about 30 keV.

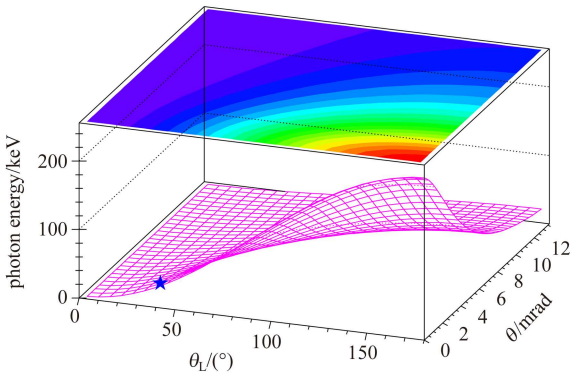


Fig. 2. The 3D-plot of LCS photon energy versus the incident angle $\theta_{\rm L}$ and the scattered angle $\theta$. The solid pentagram corresponds to on-axis X-ray energy obtained with a 1064 nm laser pulse colliding with a 112 MeV electron beam at an incident angle of 40°.

The energy spread of the LCS photon beam, $\Delta E_{\rm p}$, resulting from the uncertainties of the variables in Eq. (1) and the beam divergence of the electron beam $\theta_{\rm e}$, can be obtained by

$$\left(\frac{\Delta E_{\rm p}}{E_{\rm p}}\right)^2=\left(\frac{2\Delta E_{\rm e}}{E_{\rm e}}\right)^2+\left(\frac{\Delta E_{\rm L}}{E_{\rm L}}\right)^2+\left(\gamma\sqrt{\theta_{\rm e}^2+\theta^2}\right)^4. \tag{2}$$

Here $\Delta E_{\rm e}$ and $\Delta E_{\rm L}$ are the energy spreads of the electron and laser beams. Usually, a collimator with a small aperture is inserted downstream of the interaction point along the electron beam line. As the collimation solid angle $\theta_{\rm c}$ arising from the limited aperture is much smaller than the scattered angle $\theta$, the angle $\theta$ in Eq. (2) will be replaced by $\theta_{\rm c}$ and then the energy spread will be largely restricted. As a result, a quasi-monochromatic photon beam could be achieved by this collimator scheme. For example, the High Intensity γ-ray Source (HIγS) facility at Duke University has already generated less than 1% energy spread of the γ-ray beam at the maximum energy point by using this method [24]. But we should notice that this scheme can hardly generate an energy-tunable photon beam. In addition, the beam divergence of the electron beam has a negligible impact on the energy spread of the scattered photon beam.

The differential Compton scattering cross-section comes from the Klein-Nishina formula [25] and can be easily derived in the laboratory frame. It is

$$\frac{{\rm d}\sigma}{{\rm d}\cos\theta}=\pi r_0^2\frac{1-\beta^2}{(1-\beta\cos\theta)^2}R^2\left(R+\frac{1}{R}-1+\cos^2\theta'\right), \tag{3}$$

where $r_0$ is the classical radius of the electron,

$$R=\frac{1}{1+(1+\cos\theta')(1-\beta\cos\theta_{\rm L})\gamma\dfrac{E_{\rm L}}{m_0c^2}}$$

is the ratio between the energies of scattered and incident photons, $m_0c^2$ is the energy of electron at rest, and $\cos\theta'=\dfrac{\cos\theta-\beta}{1-\beta\cos\theta}$. Thus, for an arbitrary collision angle the energy differential cross-section of the scattered photons from Eqs. (1) and (3) is given by

$$\frac{{\rm d}\sigma}{{\rm d}E_{\rm p}}\equiv\frac{{\rm d}\sigma}{{\rm d}\cos\theta}\frac{{\rm d}\cos\theta}{{\rm d}E_{\rm p}}=\pi r_0^2R^2\left(R+\frac{1}{R}-1+\cos^2\theta'\right)\frac{\gamma^2E_{\rm e}E_{\rm L}(1-\beta)(1-\beta\cos\theta_{\rm L})-E_{\rm e}^2\beta}{\gamma^2E_{\rm L}(1-\beta\cos\theta_{\rm L})(E_{\rm L}-E_{\rm e}\beta)^2}. \tag{4}$$

The energy spectrum calculated using Eq. (4) is shown in Fig. 3. The spectrum has a high energy cutoff edge which is determined by the incident electron and photon energies. From Fig. 3, we can see that the spectral flux has a maximum value at the scaled scattering angle $\gamma\theta$=0, and a minimum value around the scaled scattering angle $\gamma\theta$=1. The ratio between them is about 2 with a negligible recoil effect. Note that almost half of the scattered photons will be radiated within a small cone of angle $\theta=1/\gamma$.

Using Eq. (4), the LCS photon yield for each collision between a laser pulse and a relativistic electron beam, $N_{\rm p}$, can be expressed with

$$N_{\rm p}^{\rm s}=L\int\frac{{\rm d}\sigma}{{\rm d}E_{\rm p}}{\rm d}E_{\rm p}, \tag{5}$$

where $L$ is the luminosity determined by the collision geometry between the electron beam and the laser pulse. In a case of collision between a laser pulse and an electron beam with Gaussian spatial distributions, the luminosity $L$ for an incident angle $\theta_{\rm L}$ is [26]

$$L=\frac{N_{\rm e}N_{\rm l}(1-\beta\cos\theta_{\rm L})}{2\pi\sqrt{\sigma_{\rm he}^2+\sigma_{\rm hp}^2}\sqrt{\sigma_{\rm wp}^2(1-\beta\cos\theta_{\rm L})^2+\sigma_{\rm we}^2(\beta-\cos\theta_{\rm L})^2+\sigma_{\rm le}^2\beta^2\sin\theta_{\rm L}^2+\sigma_{\rm lp}^2\sin\theta_{\rm L}^2}}. \tag{6}$$

Here $N_e$ is the number of electrons in the electron beam and $N_L$ is the number of photons in the laser pulse. The subscripts e and p refer to the electron and the laser; $\sigma_w$, $\sigma_h$ and $\sigma_l$ are the horizontal, vertical, and longitudinal RMS sizes, respectively. Thus, the LCS photon flux has an expression of $N_p = fN_p^s$, where $f$ is the laser and electron collision repetition rate.

The pulse width of the LCS photons can be calculated with

$$\tau_p = \frac{\sigma_{le}\sqrt{\sigma_{wp}^2(1-\beta\cos\theta_L)^2+\sigma_{we}^2(\beta-\cos\theta_L)^2+\sigma_{lp}^2\sin\theta_L^2}}{c\sqrt{\sigma_{wp}^2(1-\beta\cos\theta_L)^2+\sigma_{we}^2(\beta-\cos\theta_L)^2+\sigma_{le}^2\beta^2\sin\theta_L^2+\sigma_{lp}^2\sin\theta_L^2}}. \quad (7)$$

As a result, Eqs. (6) and (7) give the yield and temporal properties of the LCS photon beam for the slanting collision scheme. The more detailed deviation for them is presented in a companion paper [27].

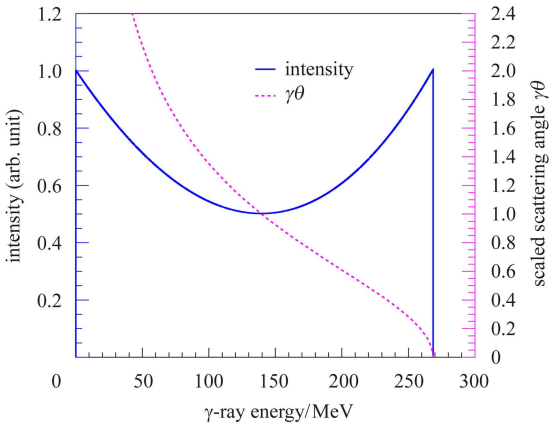


Fig. 3. The energy distribution of Compton γ-ray photons produced by a head-on collision of an 800 nm laser beam with a 3.5 GeV electron beam. The scaled scattering angle $\gamma\theta$ by the electron Lorentz factor as a function of the gamma-ray photon energy is also shown in the plot.

## 3 The laser-Compton scattering experiments at SINAP

### 3.1 The experimental setup

As described above, in order to pave the way for constructing the SLEGS beam line, a prototype Laser Electron Gamma Source (LEGS), i.e. an X-ray beam line, was established at SINAP on the high-performance 100 MeV Linac. Layout of the X-ray beam line is shown in Fig. 4. It consists mainly of the multi-angle scattering Compton chamber, the X-ray spectrometer and the remote position-control system [28], the synchronization system, the pulse-width overlapping system, the laser and optical system, the vacuum system, and the electron momentum spectrometer.

Using a Q-switched Nd:Yttrium Aluminum Garnet (YAG) laser in a pulse width of 21 and 8 ns (FWHM) and peak power of 10 and 200 MW for SINAP Ⅰ and SINAP Ⅱ, respectively, and 108 MeV electron beam bunches in 2.5 ns (FWHM) macropulse width, we have performed two principle-proof LCS experiments, i.e. SINAP Ⅰ and SINAP Ⅱ, on the prototype LEGS. Electron beam charges of about 0.1 and 0.01 nC/pulse were provided for SINAP Ⅰ and SINAP Ⅱ, respectively. In order to investigate the slanting LCS scheme, originally we designed three laser incident angles (around 40°, 90° and 140°) with regard to the electron beam which was accomplished with a facilitated LCS chamber. Given the energy response of the Si(Li) detector used to detect the produced X-rays, we chose the laser incident angle of about 40° (44°) in our experiments.

### 3.2 The critical issues for LCS experiment

To achieve the LCS processes and detect the generated X-ray spectrum, we confronted and resolved a few challenges: 1) overlapping laser and electron beam at the center of the LCS chamber, 2) synchronizing laser and electron nanosecond pulses, 3) extracting the LCS X-ray signal with a low signal to noise ratio, and 4) measuring X-ray spectrum using a method of single photon detection. For these critical issues, it is worth to mention that the first two are commom issues for LCS experiments, but the last two are necessities for us in particular since we were dedicated to obtain the photon beam spectrum. How to resolve these challenges will not be emphasized here, but one can see a detailed description in Refs. [19, 20].

### 3.3 The experimental result

First, the parameters of the 100 MeV linac and the laser system were measured. The laser and electron beam profiles were monitored with a 50 mm×50 mm size and 1 mm thick YAG plate and a 16 bit charge-coupled device camera. The measured RMS beam sizes were about 0.5 mm and 2 mm for the laser pulse

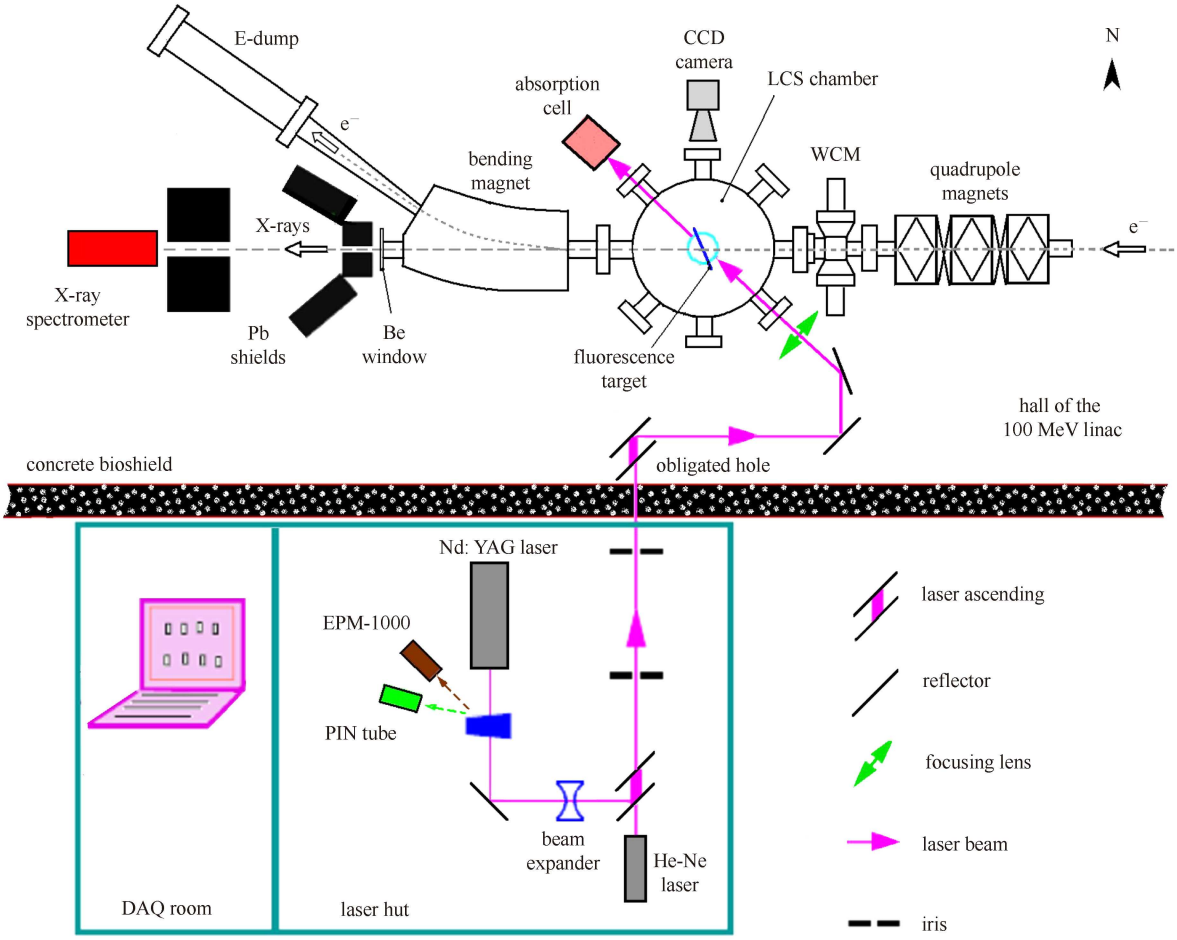


Fig. 4. Schematic of the X-ray production and measurement for SINAP Ⅰ. A similar experimental setup is employed for SINAP Ⅱ where a higher peak-power laser is used. We note the two irises are useful for fixing the optical path of the Nd:YAG laser in the laser hut.

and the electron bunch. As a result the laser and electron beam positrons were determined at the interaction point. The electron beam energy spread was measured at about 0.5% by a solid $Al_2O_3$ target following the dipole magnet. The Nd:YAG laser pulse duration (FWHM) and time jitter (RMS), $\tau_L$, were measured by p-i-n photodiode detector to be 8 ns (21 ns) and 0.9 ns (0.6 ns) for SINAP Ⅰ (SINAP Ⅱ). The electron macropulse jitter, $\tau_e$, was measured with a wall current monitor to be 0.6 ns. For a lone Nd:YAG laser pulse of the order of 10 ns (FWHM), and a 2 ns (FWHM) electron macropulse, the jitter is small and is of the order of 1 ns, and as a result, it does not appear to be a severe limitation to observe the LCS X-rays in our case. The laser energy per pulse and the electron current were measured as well. These parameters are essential for the calculation of X-ray flux described later.

During two terms experiments, the scattered LCS X-rays were detected by the same Si(Li) detector positioned downstream the interaction point about 10 meters. We note that the experimental data were taken alternatively with the laser pulse on and off. We use data with the laser pulse on minus data with the laser pulse off to separate the LCS X-ray signal from the background radiation. Although the signal to background ratio is relatively small, the generated LCS X-rays can still be observed by this method. Fig. 5 shows the X-ray energy spectrum subtracting the accumulated background. By fitting the LCS X-ray energy spectra, the peak energies of the LCS X-ray spectra are 29.1±4.9 keV and 31.7±1.7 keV for SINAP Ⅰ and SINAP Ⅱ.

From the LCS experimental result, one can also

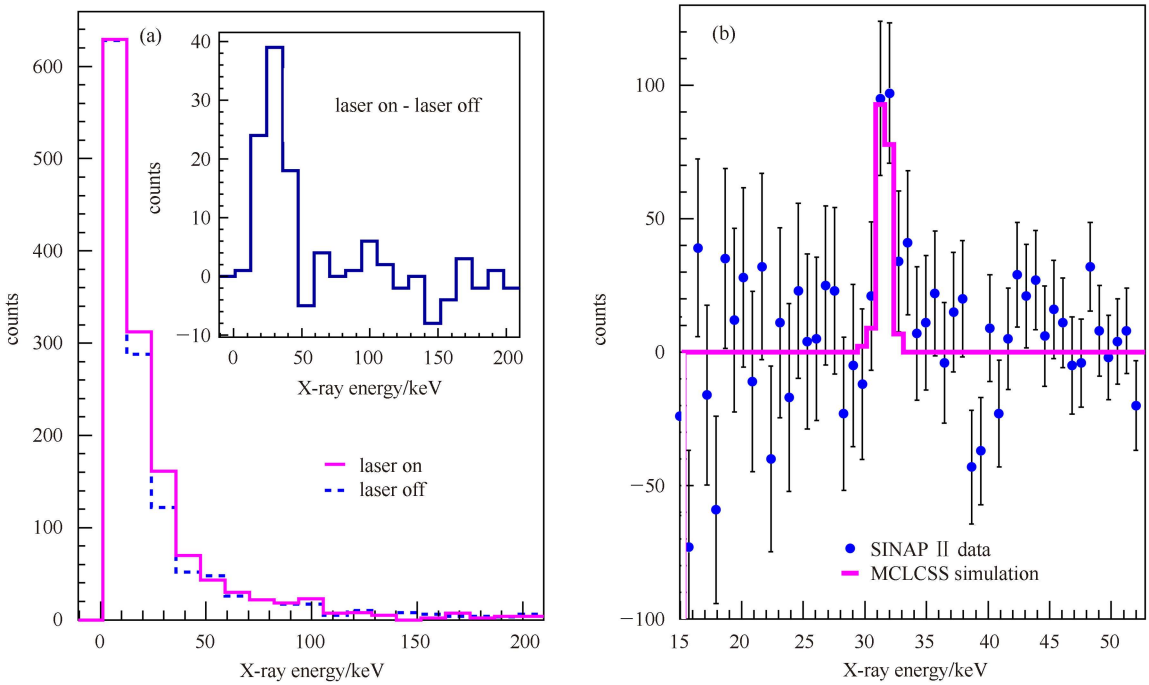


Fig. 5. The measured LCS X-ray spectra for SINAP I (a) and SINAP II (b).

determine the total LCS X-ray yield per collision and therefore calculate the LCS X-ray flux. The total LCS X-ray fluxes of 500 Hz and 50000 Hz were achieved when the 100 MeV linac and laser systems operate normally. In addition, for SINAP II we measured the LCS X-ray yield as a function of the time difference between the electron macropulse and the Nd:YAG laser pulse and the X-ray divergence angle [20].

## 4 The MCLCSS simulation

We have described two terms LCS exepriments performed at SINAP. In this section, we present our newly developed code 4D-MCLCSS for simulation of Compton scattering of a laser pulse with a relativistic electron bunch for arbitrary geometries, including the algorithm of the code 4D-MCLCSS, and its application to the X-ray production experiment at SINAP.

### 4.1 The algorithm of code MCLCSS

The code MCLCSS is mainly accomplished by employing the Compton differential cross section generalized for relativistic interactions, derived from the standard electron rest frame differential cross section and employing appropriate Lorentz transformations of the incident laser pulse into the rest frame, and of the scattered photons into the lab frame. Since the total Compton scattering cross section is as low as 665 mb, the weight method is used to improve the efficiency and to reduce the calculation time. The simulation process regarding as a combination of the following four stages is illustrated in Fig. 6 and explained as follows:

(1) initialize the electron and laser configuration by setting the electron and laser parameters and Twiss functions. After this, some pre-calculations for the slanting LCS scheme are finished and the coordinates of electrons in phase space are sampled mainly according to the Twiss parameters.

(2) simulate the Compton scattering of an electron beam with a laser beam and then produce a laser-Compton X/$\gamma$-ray beam. An arbitrary laser incident angle is employed in this stage.

(3) transport and collimate the laser-Compton X/$\gamma$-ray beam. The spectrum of the gamma-ray beam prior to the detection (namely, the incident spectrum) is obtained.

(4) transport the collimated X/$\gamma$-ray beam to the detector and simulate the interaction of the beam with the detector. After the detection, a detector response matrix and a detected spectrum are finalized.

### 4.2 Application to the laser-Compton light source

Based upon the algorithm discussed above, a 4D-MCLCSS was developed using the C++ computer language at SINAP. This code has been applied to

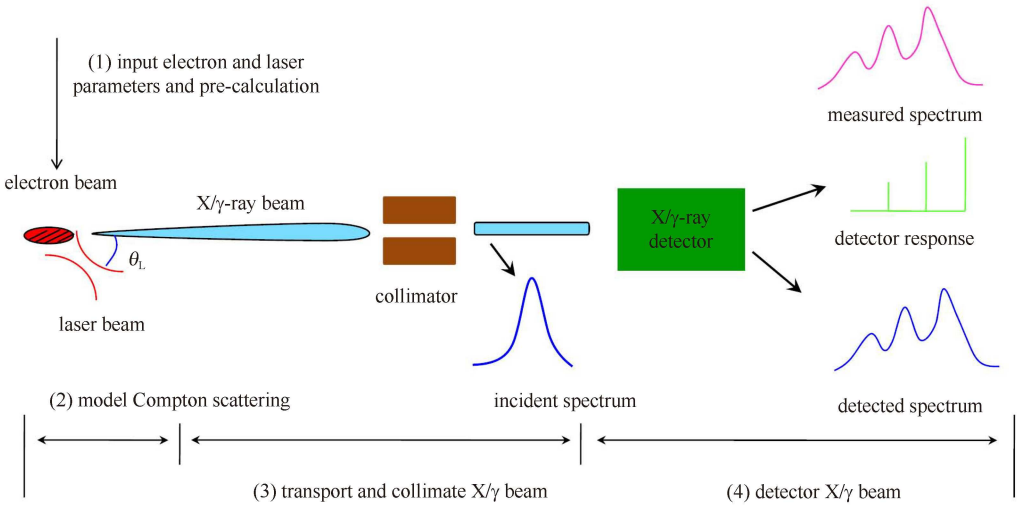


Fig. 6. Illustration of the procedures for the code MCLCSS. The laser incident angle $\theta_L$ is adjustable in our simulation.

study the characteristics of a laser-Compton light source, after being benchmarked against the experimental results from the worldwide and typical LCS facilities such as PLEIADES facility at LLNL [29] and HIγS facility at Duke university [30].

We first apply this code to reproduce the energy spectrum detecting with the Si(Li) detector for SINAP II (see Fig. 5(b)). The experimental conditions such as the electron energy spread and beam emittances, and the X-ray collimation and detection are carefully accounted for. The electromagnetic and transportation processes are properly considered with the Geant4 toolkit. One can conclude that our simulation agrees well with the measured one.

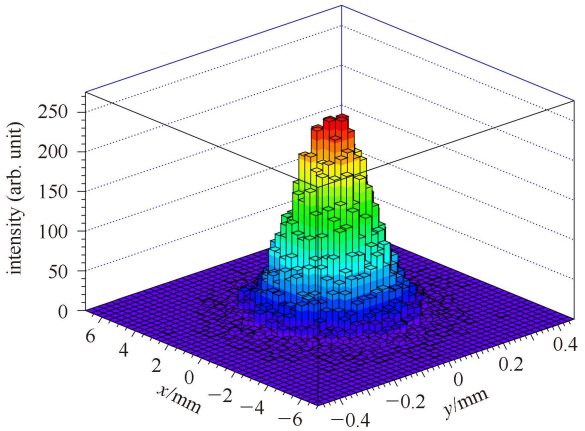


Fig. 7. The simulated spatial distribution of a laser-Compton X-ray beam in an observation plane downstream of the interaction point. The laser and electron beam parameters for simulation are borrowed from SINAP Ⅱ.

Figure 7 shows the simulated spatial distribution of a laser-Compton X-ray beam in an observation plane near the interaction point. We can see that the initial transverse sizes of the scattered photon beam are determined by both the laser and electron beams, but a very small size in $y$-direction is caused by the slanting incidence of the laser pulse. The distribution of scattered photons peaks sharply along the direction of the incident electron beam. This suggests that the X/γ-ray photons produced by the Compton scattering of a relativistic electron beam and a laser beam are mostly scattered into the electron-beam direction within a narrow cone, as demonstrated in Section 2.

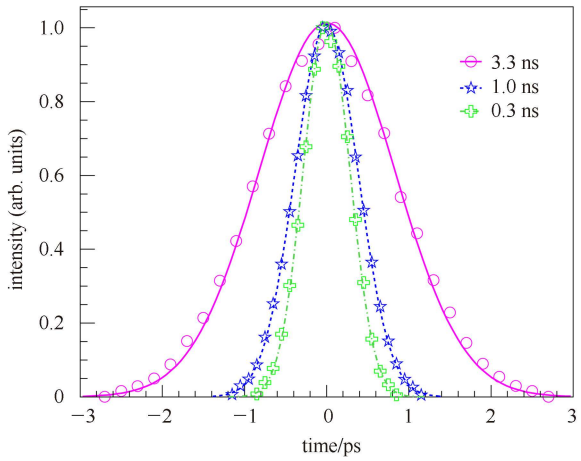


Fig. 8. Temporal pulse profiles of laser-Compton X-ray beams produced with different laser pulse durations. The pulse duration (RMS) of the laser beam is varied from 3.3 ns to 0.3 ns while the value of the electron beam is fixed to 0.9 ns.

Using the code 4D-MCLCSS, we can also study the temporal pulse profile of a laser-Compton X/γ-ray beam for a slanting geometry. Fig. 8 shows the pulse profiles of the X-ray beams produced by a 0.9 ns electron beam with different laser pulse durations. While a laser incident angle $\theta_{\rm L}$=44° is employed and laser pulse durations are set to be 3.3 ns, 1.0 ns and 0.3 ns, the corresponding scattered photon beam durations are simulated to be 0.86 ns, 0.38 ns and 0.28 ns, respectively. The simulated value, 0.86 ns, corresponds to the case of SINAP Ⅱ. It can be seen that the slanting collision scheme such as 44° geometry is useful for the generation of short-pulse X/γ-ray source, while it provides a potential for an energy-tunable photon source. This has also been explained with 90° interaction scheme in Ref. [6].

## 5 Summary and outlook

In this paper, we have demonstrated the generation of quasi-monochromatic LCS X-rays with a peak energy of about 30 keV via the interaction of Q-switched Nd:YAG laser pulses and electron macropulses at an angle of about 40°. Also we studied the spectral, spatial and temporal characteristics of an LCS X/γ-ray source by utilizing our newly developed three-dimensional time and frequency-domain Monte Carlo laser-Compton scattering simulation code. These studies will be beneficial for both the design of an energy-tunable laser-Compton light source (such as SLEGS), as well as for future experiments and applications utilizing such a source.

## References


1 Mourou G A et al. Rev. Mod. Phys., 2006, **78**: 309
2 Raubenheimer T O et al. Rev. Mod. Phys., 2000, **72**: 95
3 Compton A H. Phys. Rev., 1923, **21**: 483
4 Blumenthal G R et al. Rev. Mod. Phys., 1970, **42**: 237
5 CHEN S Y et al. Nature, 1998, **396**: 653
6 Schoenlein R W et al. Science, 1996, **274**: 236
7 Gibson D J et al. Phys. Plasmas, 2004, **11**: 2857
8 Litvinenko V N et al. Phys. Rev. Lett., 1997, **78**: 4569
9 TAN C X et al. Nucl. Instrum. Methods A, 2009, **608**: s70
10 Arthur J et al. Rev. Sci. Instrum., 1995, **66**: 1987
11 Miyamoto S et al. Radiation Measurements, 2007, **41**: S179
12 TAN C X et al. Chinese Physics C (HEP & NP), 2008, **32**: 1
13 Kudo K et al. Reactor Dosimetry: Radiation Metrology and Assessment, ASTM STP 1398, Williams J G, Wehar D W, Ruddy F H, Gilliam D M, Eds., American Society for Testing and Materials, West Conshohocken, PA, 2001
14 Robert A et al. Exp Astron, 2005, **20**: 395
15 Garrel H Von et al. Phys. Rev. C, 2006, **73**: 054315
16 Kawachi T et al. Phys. Rev. Lett., 2008, **100**: 162502
17 Pruet J et al. J. Appl. Phys., 2006, **99**: 123102
18 Ohgaki H, Kii T, Toyokawa H. IEEE Transaction on Nuclear Science, 2009, **56**: 1316
19 LUO W et al. Rev. of Sci. Instrum., 2010, **81**: 013304
20 LUO W et al. Applied Physics B, 2010, **101**: 761
21 PAN Q Y et al. Synchrotron Radiation News, 2009, **22**: 11
22 LUO W et al. Nucl. Instrum. Methods A, 2011, **660**: 108
23 Agostinelli S and Geant collaboration. Nucl. Instrum. Methods A, 2003, **506**: 250
24 Litvinenko V H, HIγS, MEGA collaborations. Nucl. Instrum. Methods A, 2003, **507**: 527
25 Klein O, Nishina Y. Z. Phys., 1929, **52**: 853
26 Kashiwagi S et al. Journal of Applied Physics, 2005, **98**: 123302
27 LUO W. Experimental Study of Laser-Compton Scattering X/γ Source and its Monte Carlo Simulation (Ph.D. thesis). Shanghai Institute of Applied Physics, Chinese Academy of Science, 2011 (in Chinese)
28 LUO W et al. Nucl. Instrum. Methods A, 2010, **624**: 141
29 Brown W J et al. Physical Review ST: Accelerators and Beams, 2004, **7**: 060702
30 SUN C, WU Y K, Rusev G, Tonchev A P. Nucl. Instrum. Methods A, 2009, **605**: 312